Numerical Investigation of In-Cylinder Cold Flow Characteristics Using Dynamic Mesh in a Compression Ignition Engine

[1]Bambhania M.P., [1]Jani D.M., [2]Jani D.S.

[1]The Maharaja Sayajirao University of Baroda, Faculty of Technology and Engineering, Mechanical Engineering Department, Vadodara, India

[2]Gyanmanjari Institute of Technology, Mechanical Engineering Department Bhavnagar, India

Abstract. The main objectives of the study are to characterize the transient cold flow structures in the cylinder of a compression ignition engine, to quantify how piston motion changes these structures relative to a fixed geometry, and to determine the pressure and temperature histories of the motored cycle as a baseline for subsequent combustion modeling. These objectives were achieved by building a two-dimensional computational model of a single-cylinder production engine with a bore of 95 mm, a stroke of 110 mm and a compression ratio of 15.5 (the effective volume ratio of the planar model is 12), and by solving the unsteady compressible conservation equations with a pressure-based solver and the standard k–epsilon turbulence model; piston motion was represented by a layering and spring-smoothing moving-mesh technique, and three cases were simulated: intake with fixed geometry, intake and exhaust with a moving piston, and motored compression and expansion. The most important results are that the fixed-geometry intake produced a single dominant toroidal vortex, whereas the moving piston produced one dominant clockwise vortex with two smaller counter-rotating vortices and a markedly asymmetric flow, that the exhaust stroke left residual vortical structures in the cylinder, and that motored compression reached a peak gauge pressure of 3.18 MPa and a peak temperature of 808.6 K near top dead centre, accompanied by organized tumble and recirculation zones. The significance of the obtained results lies in showing that neglecting piston motion misrepresents the in-cylinder vortex structure, and in providing a mesh-independent motored baseline on which fuel injection, combustion and emission models can be built.

Keywords: moving mesh; layering; piston kinematics; tumble; toroidal vortex; motored cycle; turbulence modeling; pressure–volume diagram.

DOI: https://doi.org/10.52254/1857-0070.2026.4-72.14
UDC: 621.436

Investigarea numerică a caracteristicilor curgerii reci în cilindru utilizând rețea dinamică într-un motor cu aprindere prin comprimare

[1]Bambhania M.P., [1]Jani D.M., [2]Jani D.S.

[1]Universitatea Maharaja Sayajirao din Baroda, Facultatea de Tehnologie și Inginerie, Departamentul de Inginerie Mecanică, Vadodara, India

[2]Institutul de Tehnologie Gyanmanjari, Departamentul de Inginerie Mecanică Bhavnagar, India

Rezumat. Obiectivele principale ale studiului sunt caracterizarea structurilor tranzitorii ale curgerii reci în cilindrul unui motor cu aprindere prin comprimare, cuantificarea modului în care mișcarea pistonului modifică aceste structuri față de cazul unei geometrii fixe și determinarea evoluției presiunii și temperaturii în ciclul antrenat, ca bază pentru modelarea ulterioară a arderii. Aceste obiective au fost atinse prin elaborarea unui model computațional bidimensional al unui motor monocilindric de serie, cu alezajul de 95 mm, cursa de 110 mm și raportul de comprimare de 15.5 (raportul efectiv al volumelor în modelul plan este de 12), precum și prin rezolvarea ecuațiilor nestaționare de conservare pentru un fluid compresibil, utilizând un solver bazat pe presiune și modelul standard de turbulență k–ε. Cele mai importante rezultate constau în faptul că admisia în cazul geometriei fixe a generat un singur vortex toroidal dominant, în timp ce mișcarea pistonului a generat un vortex dominant în sensul acelor de ceasornic, însoțit de două vortexuri mai mici care se rotesc în sens opus, precum și o curgere pronunțat asimetrică. De asemenea, la sfârșitul cursei de evacuare, în cilindru au rămas structuri vorticale reziduale, iar în timpul comprimării antrenate s-au atins, în apropierea punctului mort superior, o presiune manometrică maximă de 3.18 MPa și o temperatură maximă de 808.6 K. Semnificația rezultatelor obținute constă în demonstrarea faptului că neglijarea mișcării pistonului denaturează structura vorticală din cilindru și în furnizarea unei baze de referință independente de rețea pentru ciclul antrenat, pe baza căreia pot fi dezvoltate ulterior modele de injecție a combustibilului, de ardere și de formare a emisiilor.

© Bambhania M.P., Jani D.M., Jani D.S. 2026

Cuvinte-cheie: rețea mobilă; stratificare; cinematica pistonului; mișcare de tip tumble; vortex toroidal; ciclu antrenat; modelarea turbulenței; diagramă presiune–volum.

Численное исследование характеристик холодного течения в цилиндре двигателя с воспламенением от сжатия с использованием динамической сетки

[1]Бамбхания М.П., [1]Джани Д.М., [2]Джани Д.С.

[1]Университет Махараджи Саяджирао в Бароде, факультет технологии и инженерии, кафедра машиностроения, Вадодара, Индия

[2]Технологический институт Гьянманджари, кафедра машиностроения Бхавнагар, Индия

Аннотация. Основными целями исследования являются описание нестационарных структур холодного течения в цилиндре двигателя с воспламенением от сжатия, количественная оценка того, как движение поршня изменяет эти структуры по сравнению с неподвижной геометрией, а также определение изменения давления и температуры в цикле прокрутки как основы для последующего моделирования горения. Цели были достигнуты путём построения двумерной расчётной модели одноцилиндрового серийного двигателя с диаметром цилиндра 95 мм, ходом поршня 110 мм и степенью сжатия 15.5 (эффективное отношение объёмов плоской модели равно 12) и решения нестационарных уравнений сохранения для сжимаемой среды с помощью решателя, основанного на давлении, и стандартной модели турбулентности k–эпсилон; движение поршня описывалось методом подвижной сетки с послойным добавлением и удалением ячеек и пружинным сглаживанием, при этом были рассчитаны три случая: впуск при неподвижной геометрии, впуск и выпуск с движущимся поршнем, а также сжатие и расширение в режиме прокрутки. Наиболее важные результаты заключаются в том, что при неподвижной геометрии впуск формирует один доминирующий тороидальный вихрь, тогда как при движущемся поршне образуются один доминирующий вихрь, вращающийся по часовой стрелке, и два меньших вихря противоположного вращения, а течение становится асимметричным; что к концу такта выпуска в цилиндре сохраняются остаточные вихревые структуры; и что при сжатии в режиме прокрутки вблизи верхней мёртвой точки достигаются максимальное избыточное давление 3.18 МПа и максимальная температура 808.6 К, сопровождаемые упорядоченным движением типа «тамбл» и зонами рециркуляции. Значимость полученных результатов состоит в демонстрации того, что пренебрежение движением поршня искажает вихревую структуру течения в цилиндре, а также в получении не зависящей от сетки базовой картины цикла прокрутки, на основе которой могут строиться модели впрыска топлива, горения и образования выбросов.

Ключевые слова: подвижная сетка; послойный метод; кинематика поршня; движение типа «тамбл»; тороидальный вихрь; цикл прокрутки; моделирование турбулентности; диаграмма давление–объём.

I. INTRODUCTION

The demand for higher efficiency and lower emissions from internal combustion engines has made a detailed understanding of in-cylinder flow dynamics essential. In compression ignition (CI) engines, the bulk air motion, the turbulence intensity and the quality of fuel–air mixing largely govern the combustion process [1]. These transient phenomena can be captured experimentally only under limited conditions, especially in production engines without optical access. Computational fluid dynamics (CFD) has therefore become a key tool for examining in-cylinder processes and for supporting engine design.

Several studies have addressed the in-cylinder air motion directly. Payri et al. [2] computed the intake and compression strokes of a four-valve direct-injection diesel engine and compared the results with laser Doppler velocimetry measurements; the model was reasonably accurate around top dead center, but turbulence was under-predicted where squish effects were strong. Murali Krishna and Mallikarjuna [3] measured tumble flows in a motored single-cylinder engine with five piston crown shapes by particle image velocimetry and found that the crown shape strongly affects the tumble ratio and the turbulent kinetic energy at the end of compression. Gnana Sagaya Raj et al. [4] reproduced such measurements numerically for four piston configurations, and Perini et al. [5] validated full induction-stroke calculations against velocity fields measured in an optical light-duty diesel engine. Taghavifar et al. [6] showed that the piston bowl geometry changes the flow field and the turbulent kinetic energy

and, consequently, the combustion and performance characteristics.

A second group of CFD studies has concentrated on fuel injection and spray formation, because they strongly affect the subsequent combustion. Nozzle flow and cavitation in diesel injectors have been shown to influence atomization and fuel–air contact [7], the modeling of primary breakup has been linked to spray and combustion behavior [8], and numerical and experimental studies of high-pressure diesel sprays have clarified momentum flux and jet formation [9] as well as spray tip penetration and radial expansion under reacting conditions [10]. With the development of homogeneous charge compression ignition (HCCI), premixed charge compression ignition (PCCI) and reactivity-controlled compression ignition (RCCI), dual-fuel combustion with in-cylinder fuel blending has been shown to control combustion phasing and efficiency [11, 12], the effects of injection timing and blending ratio on RCCI combustion have been quantified [13], and RCCI has been reviewed as a pathway to high-efficiency, low-emission combustion [14]. Large eddy simulation (LES) has improved the prediction of spray and combustion characteristics under engine-like conditions [15], although Reynolds-averaged Navier–Stokes (RANS) models remain the practical choice for engine simulations because of their lower computational cost. Studies of hydrogen-fuelled engines have further highlighted the role of in-cylinder flow in combustion behavior [16].

More recent work has extended CFD to multi-component fuels and advanced combustion strategies, including spray combustion, soot formation and emissions of ternary diesel–biodiesel–gasoline mixtures [17] and the effect of injection timing on biodiesel combustion and emissions [18]. A recent review has emphasized that accurate turbulence–chemistry interaction models are required to improve the predictive power of engine CFD [19]. Simulations of pre-chamber ignition in a large-bore engine [20] and of e-fuels and syngas in a spark ignition engine [21], both validated against experiments, have confirmed the ability of CFD to predict engine performance and combustion.

Despite this progress, several gaps remain. Most of the studies cited above either concentrate on sprays and combustion [7–21] or evaluate the in-cylinder flow for a given piston or port design with full three-dimensional models [2–6]. The isolated effect of the moving piston itself, that is, the difference between a fixed-geometry solution and a moving-boundary solution for the same cylinder under identical inlet conditions, is rarely reported, and the link between the resulting vortex structures and the thermodynamic state of the motored charge is seldom shown within a single consistent model. Cold flow simulation, which excludes chemical reactions, is well suited to isolating these aerodynamic effects, but it requires a moving-mesh treatment of the piston that preserves mesh quality over the whole stroke.

The present study addresses these gaps with a two-dimensional dynamic mesh model of a single-cylinder CI engine. Its objectives are: (1) to establish the baseline intake flow structure in a fixed geometry; (2) to quantify how piston motion, represented by a layering dynamic mesh, modifies the vortex structures during the intake and exhaust strokes; and (3) to determine the pressure, temperature and flow-structure evolution during motored compression and expansion and to check them against thermodynamic expectations. The novelty of the work lies in the direct comparison of fixed and moving-boundary solutions for the same geometry and in the combination of flow-structure and thermodynamic analysis within one motored-cycle model. All models, simulations and results presented in Sections II and III are the authors' own; published data are used only for comparison in Section III-F.

II. NUMERICAL METHODOLOGY

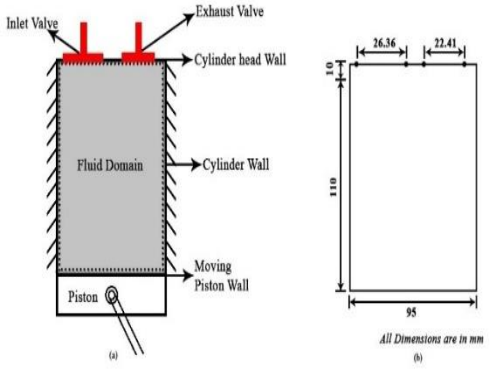
A. Computational Domain

The computational domain is a two-dimensional section of the cylinder of a single-cylinder CI engine, constructed from the dimensions of a production engine (Table 1). The domain includes the cylinder head wall with the inlet and exhaust valve openings, the cylinder wall and the moving piston wall (Fig. 1). The simulation starts with the piston at bottom dead center (BDC), where the cylinder volume is largest, and the domain contains both the clearance volume and the swept volume so that the complete cycle can be represented. In the planar model, the volume per unit depth is proportional to the height of the gas column, so the volume ratio equals (clearance height + stroke)/clearance height. The clearance height used in the simulations was 10 mm, which gives an effective volume ratio of 12; reproducing the compression ratio of 15.5 of the production engine would require a clearance height of

110/(15.5 − 1) ≈ 7.6 mm. The effect of this difference on the computed peak pressure and temperature is quantified in Section III-F.

Table 1 Specifications of the compression ignition engine used for numerical modeling

Parameter	Value
Engine type	Single-cylinder, four-stroke CI engine
Bore	95 mm
Stroke	110 mm
Displacement volume	780 cm^3
Compression ratio	15.5 (production engine); 12 (effective volume ratio of the 2-D model)
Speed	749 min^{-1}



(a) schematic of the domain and boundaries; (b) main dimensions, mm.

Fig. 1. Computational domain of the compression ignition engine.

B. Mesh Generation

The domain was discretized with a structured quadrilateral mesh generated by face meshing, which produces the layered cell arrangement required by the dynamic layering method (Fig. 2). The mesh was refined near the piston, the walls and the valve openings to resolve the steep flow gradients there.

Mesh independence was assessed with three meshes of 2322, 20898 and 37152 cells (Fig. 2). The in-cylinder pressure histories obtained with the three meshes are compared in Fig. 3. The differences between the medium and fine meshes are negligible; therefore, the medium mesh was used for all further calculations as a compromise between accuracy and computational cost.

C. Governing Equations

The in-cylinder flow is described by the unsteady compressible equations of conservation of mass, momentum and energy:

$$\frac{\partial \rho}{\partial t} + \nabla \cdot (\rho \mathbf{u}) = 0 \tag{1}$$

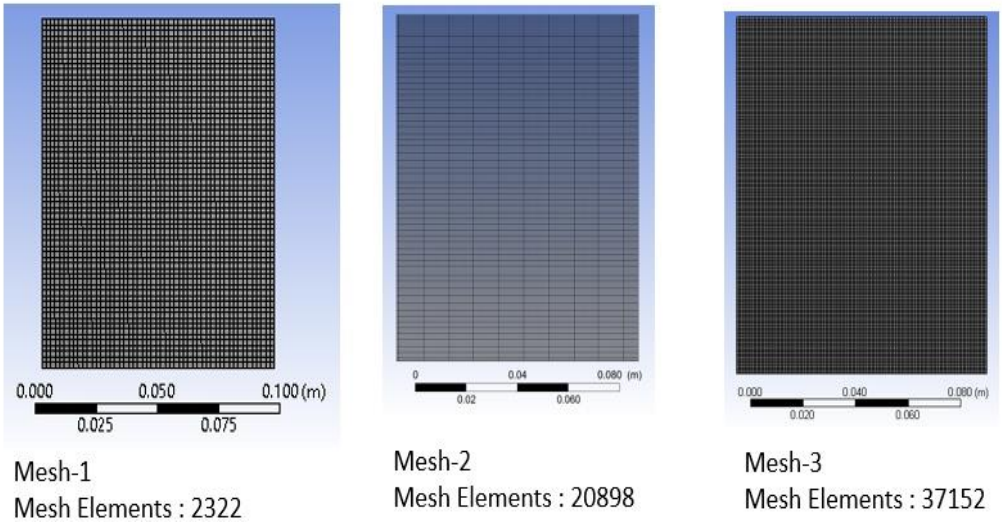
$$\frac{\partial (\rho \mathbf{u})}{\partial t} + \nabla \cdot (\rho \mathbf{u}\mathbf{u}) = -\nabla p + \nabla \cdot \tau \tag{2}$$

$$\frac{\partial (\rho E)}{\partial t} + \nabla \cdot \left[\mathbf{u} (\rho E + p) \right] = \nabla \cdot (\lambda \nabla T) + \Phi \tag{3}$$

The air is treated as an ideal gas:

$$p = \rho R T \tag{4}$$

where ρ — density; **u** — velocity vector; p — pressure; τ — viscous stress tensor; E — total specific energy; λ — thermal conductivity; T — temperature; Φ — viscous dissipation term; R — specific gas constant of air.



Mesh-1 — 2322 cells; Mesh-2 — 20898 cells; Mesh-3 — 37152 cells.

Fig. 2. Structured quadrilateral meshes of the computational domain at bottom dead center used in the mesh independence study.

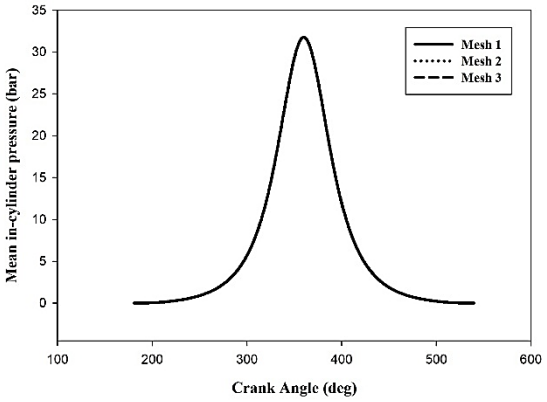


Fig. 3. Mesh independence study: in-cylinder pressure versus crank angle for the coarse, medium and fine meshes.

D. Turbulence Modeling

Turbulence is modeled with the standard k–ε model [22], which is robust and widely used for engine flows. The transport equations for the turbulent kinetic energy k and its dissipation rate ε are:

$$\frac{\partial(\rho k)}{\partial t}+\nabla\cdot(\rho k\mathrm{u})=\nabla\cdot(\mu_{\mathrm{eff}}\nabla k)+G_k-\rho\varepsilon \quad (5)$$

$$\frac{\partial(\rho\varepsilon)}{\partial t}+\nabla\cdot(\rho\varepsilon\mathrm{u})=\nabla\cdot(\mu_{\mathrm{eff}}\nabla\varepsilon)+C_{1\varepsilon}\frac{\varepsilon}{k}G_k-C_{2\varepsilon}\rho\frac{\varepsilon^2}{k} \quad (6)$$

where μ_{eff} — effective viscosity, $\mu_{\mathrm{eff}}=\mu+\mu_t/\sigma$, with $\sigma=\sigma_k$ in Equation 5 and $\sigma=\sigma_\varepsilon$ in Equation 6; μ — molecular viscosity; $\mu_t=\rho C_\mu k^2/\varepsilon$ — turbulent viscosity; G_k — production of turbulent kinetic energy by the mean velocity gradients; $C_{1\varepsilon}$, $C_{2\varepsilon}$, C_μ, σ_k, σ_ε — model constants, taken with their standard values of 1.44, 1.92, 0.09, 1.0 and 1.3, respectively [22].

E. Dynamic Mesh Formulation

Piston motion is represented by the dynamic layering method: the cell layer adjacent to the piston is split when its height exceeds a threshold and collapsed when its height falls below one, while spring-based smoothing preserves the quality of the interior mesh during deformation. The dynamic mesh parameters are listed in Table 2.

Table 2 Dynamic mesh parameters used for piston motion modeling

Parameter	Value
Smoothing method	Spring-based
Layering method	Enabled
Split factor	0.4
Collapse factor	0.4

The piston position is prescribed as a function of crank angle by the slider–crank relation:

$$x_p=\frac{S}{2}(1-\cos\theta)+L\left[1-\sqrt{1-\left(\frac{r}{L}\sin\theta\right)^2}\right] \quad (7)$$

where x_p — piston displacement from top dead center (TDC); S — stroke; L — connecting rod length; r — crank radius, $r = S/2$; θ — crank angle. The crank angle is related to the flow time by

$$\theta=\omega t+\theta_0 \quad (8)$$

where ω — angular velocity of the crankshaft, equal to 78.4 rad/s at 749 min^{-1}; t — time; θ_0 — initial crank angle.

F. Boundary and Initial Conditions

The simulations were performed with the pressure-based transient solver of ANSYS Fluent. Air is treated as an ideal gas, and gravity acts in the negative vertical direction. All walls are no-slip; the piston wall is a moving boundary that follows Equation 7, so that the time-varying cylinder volume is reproduced throughout the cycle. The boundary and initial conditions are summarized in Table 3. The intake and exhaust valves are represented by fixed, fully open slots 26.36 mm and 22.41 mm wide (Fig. 1b) that extend over the whole depth of the planar domain; valve lift and the valve discharge coefficient are not modeled. A constant mass flow rate (Table 3) is imposed at the intake slot throughout the intake stroke, so the pressure difference across the intake valve is not resolved, and the pressure outlet (0 Pa gauge) is placed directly at the exhaust valve plane, without an exhaust port or exhaust system.

Table 3Boundary and initial conditions used in the simulations

Parameter	Value
Initial temperature	300 K
Initial pressure	101 325 Pa
Wall temperature	300 K
Inlet mass flow rate	$7.244\cdot10^{-4}$ kg/s (constant)
Turbulence intensity	5 %
Turbulent viscosity ratio	10
Outlet	Pressure outlet, 0 Pa gauge, at the exhaust valve plane

G. Simulation Cases

Three cases were simulated, each isolating one physical effect. In the first case, the intake flow was computed in a fixed geometry without piston motion; this case provides the baseline flow development and vortex formation at BDC against which the other cases are compared. In the second case, piston motion was included through the dynamic mesh, and the intake and exhaust strokes were computed over the corresponding crank-angle ranges; this case shows how the moving boundary changes the vortex dynamics and the flow structures. In the third case, the compression and expansion strokes were computed under cold flow conditions without fuel injection or combustion, which isolates the fluid-dynamic and thermodynamic behavior of the charge.

III. RESULTS AND DISCUSSION

A. In-Cylinder Flow without Dynamic Mesh

The fixed-geometry case establishes the flow development without piston motion. During intake, the incoming air enters the cylinder as a jet, impinges on the lower wall and is redirected along the cylinder walls (Fig. 4). The velocity vectors illustrate the presence of a pronounced recirculation region in the upper part of the cylinder, generated through the interaction between the jet and the confining walls and which redistributes the momentum and increases the local turbulence.

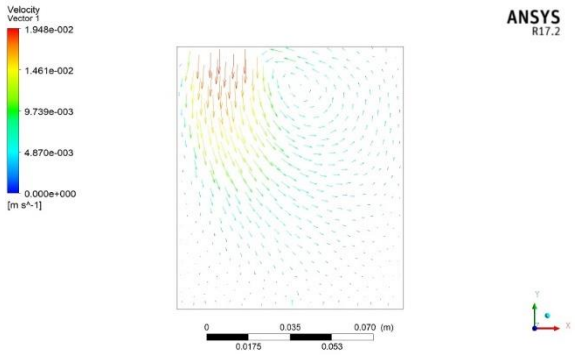


Fig. 4. Velocity vectors of the in-cylinder flow without dynamic mesh at bottom dead center.

The streamlines in Fig. 5 show that a single large toroidal vortex occupies most of the cylinder volume. This vortex promotes recirculation and mixing in the cylinder and serves as the reference for assessing the effect of piston motion in the following subsections.

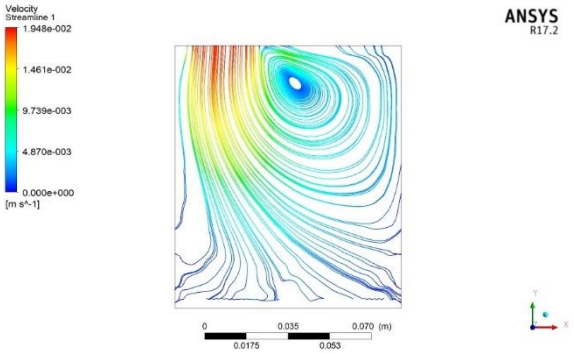


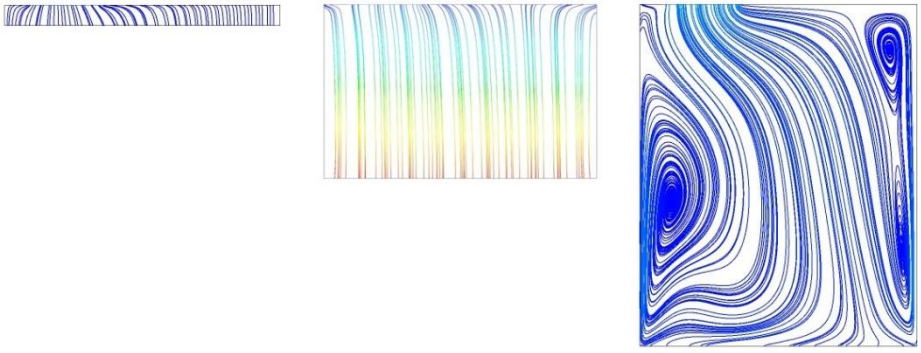
Fig. 5. Streamlines of the in-cylinder flow without dynamic mesh, showing the toroidal vortex.

B. Effect of Dynamic Mesh on In-Cylinder Flow

Due to the dynamic mesh, the in-cylinder flow field is significantly altered by the piston motion and the dynamic interaction between the intake jet and the moving piston creates flow patterns that vary with the crank angle.

1) Intake Stroke

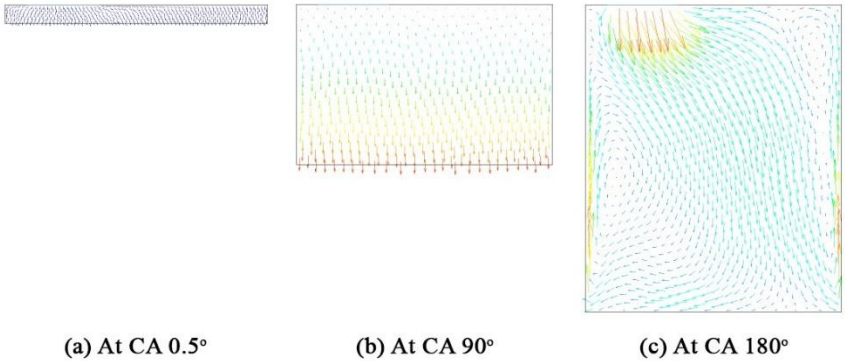
The development of the flow during the intake stroke is shown by the streamlines in Fig. 6. At small crank angles (Fig. 6a), the flow is dominated by jet penetration through the intake valve. As the piston descends, the flow impinges on the cylinder wall, is deflected and forms vortical structures (Fig. 6b). Towards the end of the intake stroke, several vortices are present in the cylinder (Fig. 6c).



(a) θ = 0.5°, initial jet penetration; (b) θ = 90°, wall interaction and vortex formation; (c) θ = 180°, multi-vortex structure near BDC.

Fig. 6. Evolution of in-cylinder streamlines during the intake stroke.

The velocity vectors in Fig. 7 show that the combined effect of the jet momentum and the piston motion concentrates high-velocity regions near the piston (Fig. 7b). In the later stages (Fig. 7c), three vortices have formed: one dominant clockwise vortex and two smaller counter-rotating vortices. The flow is therefore considerably more complex and asymmetric than in the fixed-geometry case, where only one toroidal vortex was found.

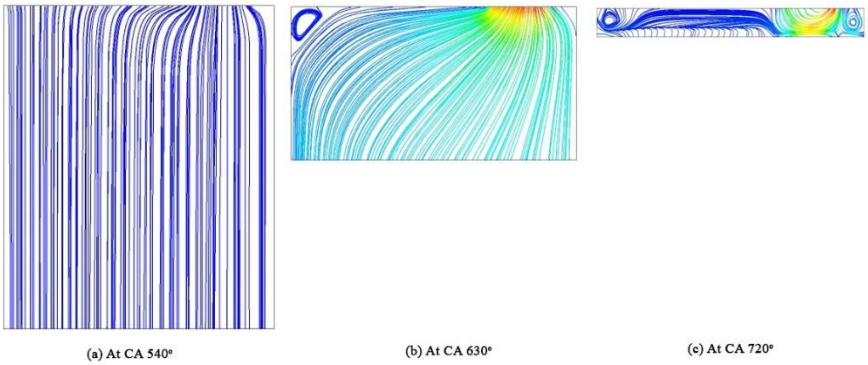


(a) θ = 0.5°, initial jet penetration; (b) θ = 90°, wall interaction and vortex formation; (c) θ = 180°, multi-vortex structure near BDC.

Fig. 7. Evolution of in-cylinder velocity vectors during the intake stroke.

2) Exhaust Stroke

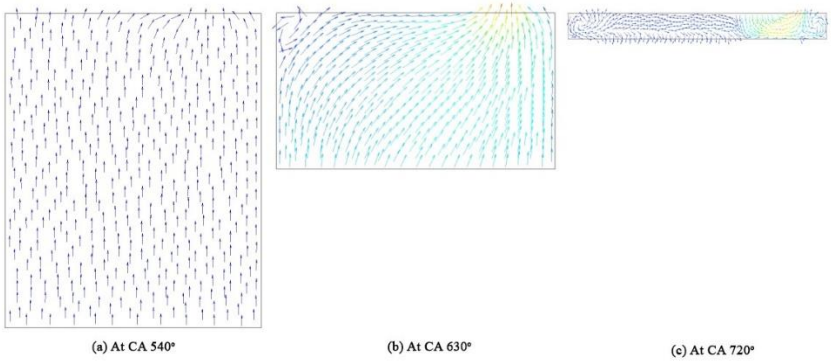
During the exhaust stroke, the gases are expelled through the exhaust valve under the combined action of the pressure gradient and the rising piston. The streamlines in Fig. 8 show that the flow converges towards the exhaust valve. At the beginning of the stroke (Fig. 8a), the flow starts to turn towards the exhaust port; as the piston velocity increases, the outflow accelerates and a strong jet form at the valve exit (Fig. 8b); towards the end of the stroke, vortical structures still remain in the cylinder (Fig. 8c).



(a) θ = 540°; (b) θ = 630°; (c) θ = 720°.

Fig. 8. Evolution of in-cylinder streamlines during the exhaust stroke.

The velocity vectors in Fig. 9 show concentrated high-velocity regions around the exhaust valve, indicating effective evacuation of the gases, while residual flow structures remain near the intake side, which shows that the vortices formed during the preceding strokes have not fully dissipated.



(a) θ = 540°; (b) θ = 630°; (c) θ = 720°.

Fig. 9. Evolution of in-cylinder velocity vectors during the exhaust stroke.

The mean in-cylinder pressure during the exhaust stroke (Fig. 10) first rises owing to the displacement of the charge by the piston, reaches a maximum of about 11 Pa above atmospheric near 600° crank angle and then falls as the gases leave the cylinder. This trend reflects the interaction between the piston motion and the outflow. The magnitude of this pressure is, however, much smaller than in a real engine, where the cylinder pressure during the exhaust stroke exceeds the atmospheric pressure by the order of 10^3–10^4 Pa. The small value is a consequence of the idealized exhaust boundary (Section II-F): the exhaust valve is a permanently open slot with a flow area of 0.0224 m² per metre of depth, i.e. about 24 % of the piston area, and the pressure outlet is placed directly at the valve plane, so the throttling of the flow by the valve curtain area and the back-pressure of the exhaust port and exhaust system are not represented. Fig. 10 therefore shows only the qualitative trend of the cylinder pressure during the exhaust stroke and is not used for quantitative conclusions.

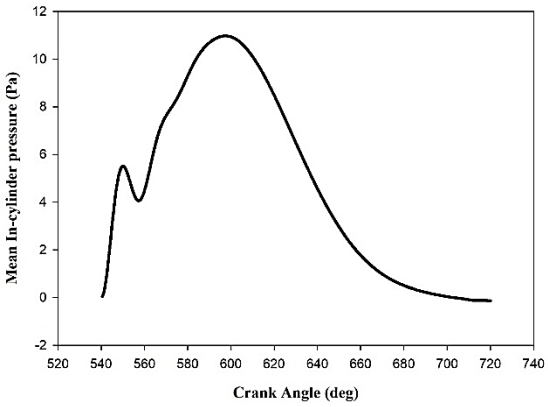
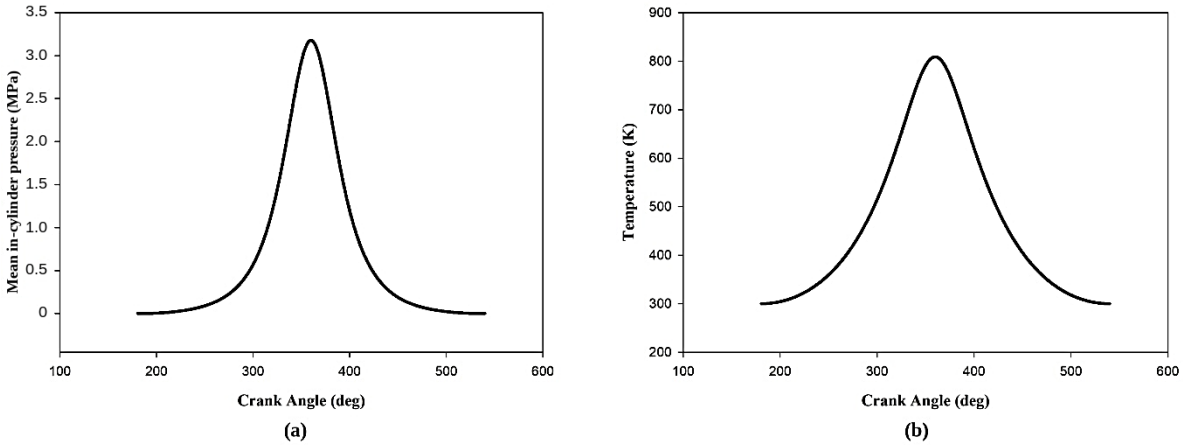


Fig. 10. Mean in-cylinder gauge pressure versus crank angle during the exhaust stroke.

C. Thermodynamic Behavior under Cold Flow Conditions

The motored simulation shows how the charge evolves thermodynamically during

compression and expansion without combustion. The pressure rises continuously during the compression stroke as the cylinder volume decreases (Fig. 11a) and reaches a maximum gauge pressure of 3.176 MPa near TDC. The temperature rises correspondingly to a maximum of 808.6 K (Fig. 11b). Both curves are nearly symmetric about TDC, as expected in the absence of combustion. The peak temperature is well above the auto-ignition temperature of diesel fuel, which confirms that the motored conditions are representative of those at the start of injection in a CI engine.



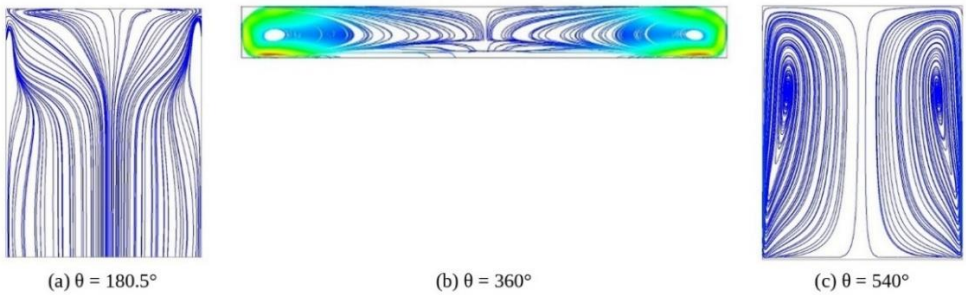
(a) gauge pressure; (b) temperature.

Fig. 11. In-cylinder gauge pressure and temperature versus crank angle during motored compression and expansion.

D. Flow Structure Evolution during Compression and Expansion

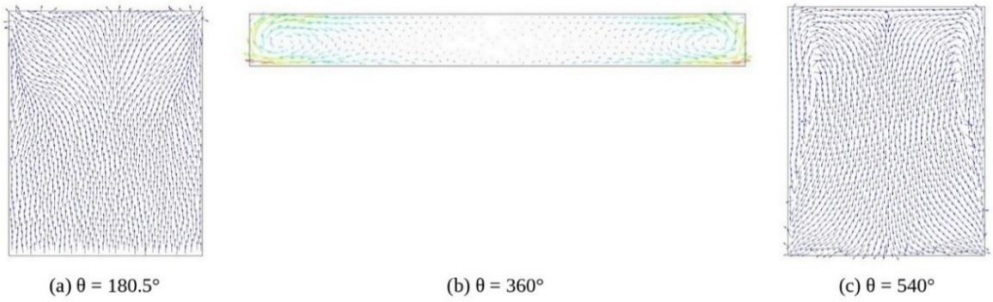
The transient flow field during compression and expansion shows how turbulence is generated and enhanced. Because the mean piston speed (2.75 m/s) is very small compared with the speed of sound, the pressure in the cylinder is practically uniform at every crank angle: the computed spatial pressure differences do not exceed a few hundred pascals, i.e. less than 0.2 % of the absolute in-cylinder pressure. The in-cylinder pressure is therefore fully characterized by its mean value (Fig. 11a), and the discussion below concentrates on the velocity and temperature fields.

The streamlines in Fig. 12 show the development of tumble motion. As the piston approaches TDC, the flow is compressed and deflected, and large-scale vortical structures develop. The velocity vectors in Fig. 13 show the interaction of counter-rotating vortices, which increases the turbulence intensity and mixing; such structures are important for the subsequent mixture formation and combustion.



(a) θ = 180.5°; (b) θ = 360°; (c) θ = 540°.

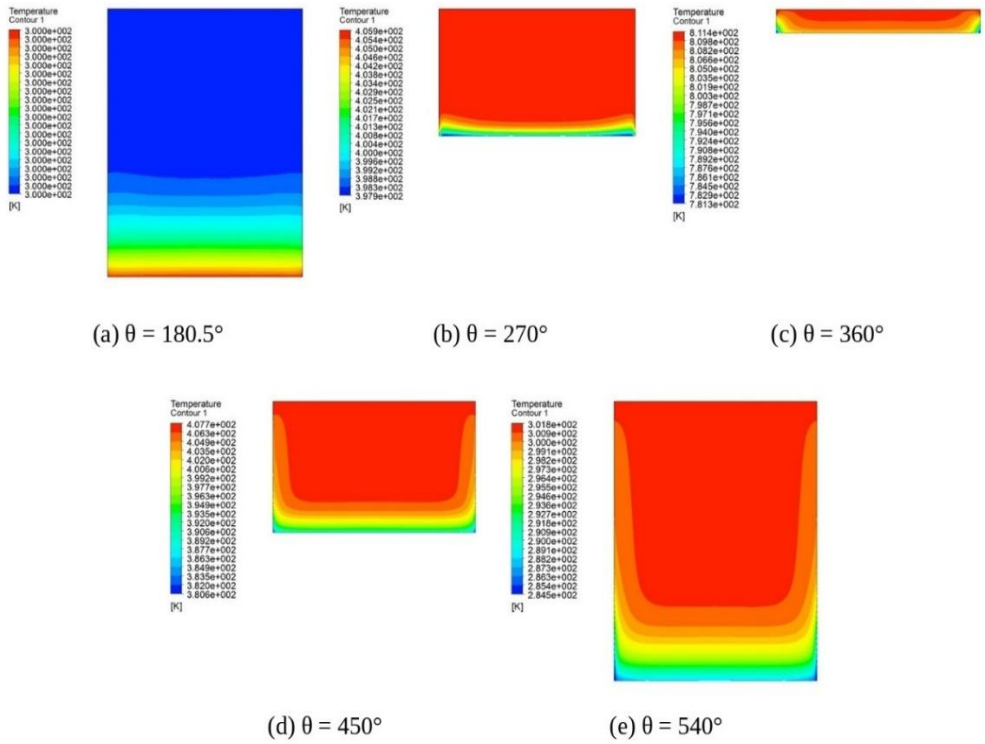
Fig. 12. Streamlines showing the development of tumble motion during compression and expansion.



(a) θ = 180.5°; (b) θ = 360°; (c) θ = 540°.

Fig. 13. Velocity vectors showing vortex interaction and the development of turbulent flow structures during compression and expansion.

The temperature contours in Fig. 14 show that the core of the charge has a practically uniform temperature during compression and expansion, while thin layers adjacent to the piston, the cylinder wall and the cylinder head, which are kept at 300 K, are cooler than the core by up to about 30 K (Fig. 14b–e); these near-wall layers are the thermal boundary layers produced by heat transfer to the walls. At θ = 180.5° (Fig. 14a), the whole charge is at 300 K, and the colored bands correspond to temperature differences below 0.1 K that result only from the automatic scaling of the color legend.

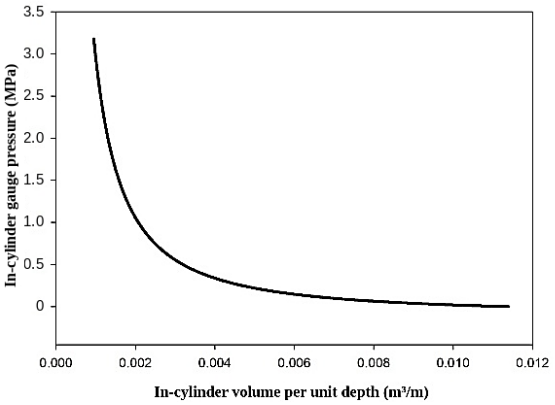


(a) θ = 180.5°; (b) θ = 270°; (c) θ = 360°; (d) θ = 450°; (e) θ = 540°.

Fig. 14. Temperature contours at different crank angles during compression and expansion.

E. Pressure–Volume Analysis

The pressure–volume (p–V) diagram of the motored cycle is shown in Fig. 15, where the volume is given per unit depth of the two-dimensional domain. Without combustion, the compression and expansion curves coincide: the pressure rises as the volume decreases during compression and falls along the same path during expansion. The volume varies from about 0.0114 m³/m at BDC to about 0.00095 m³/m at TDC; the effective volume ratio of the two-dimensional domain is therefore about 12, lower than the compression ratio of 15.5 of the production engine, because the clearance height of the planar model was not adjusted to preserve the compression ratio (Section II-A).



Gauge pressure; volume per unit depth of the 2-D domain.

Fig. 15. Pressure–volume diagram of the motored cycle.

F. Relation of Results to Objectives and Comparison with Previous Work

Objective 1 was addressed by the fixed-geometry case (Figs. 4 and 5). The intake jet produced a single large toroidal vortex occupying most of the cylinder, which defines the baseline flow structure.

Objective 2 was addressed by the dynamic mesh cases (Figs. 6–10). The most significant result of the study is that piston motion changes the flow topology qualitatively: instead of one toroidal vortex, one dominant clockwise vortex and two smaller counter-rotating vortices formed during intake, and the flow became markedly asymmetric. During the exhaust stroke, the flow was dominated by a high-velocity jet at the exhaust valve, and residual vortices remained in the cylinder at the end of the stroke. A fixed-geometry model would therefore misrepresent the flow structure that is carried over into the next cycle.

Objective 3 was addressed by the motored compression–expansion case (Figs. 11–15). The peak gauge pressure and temperature were 3.176 MPa and 808.6 K near TDC, organized tumble motion and recirculation zones formed during compression, and the compression and expansion curves of the p–V diagram coincided. For comparison, ideal isentropic compression of air with the ratio of specific heats of 1.4 from 101 325 Pa and 300 K at the effective volume ratio of the model, 12, gives 3.184 MPa (gauge) and 810.6 K. The simulated values differ from these by only 0.2 %, and the effective polytropic exponent derived from both the pressure and the temperature rise, n = 1.40, equals the isentropic value. This agreement verifies the thermodynamic consistency of the dynamic mesh solution; it also shows that heat losses are negligible in the model, whereas polytropic exponents of about 1.3 are typically observed in real engines [1] because of heat transfer and blow-by. Applying the same isentropic relation at the compression ratio of the production engine, 15.5, gives about 4.60 MPa (gauge) and 898 K. The peak values computed with the planar model are therefore about 31 % (pressure) and 10 % (temperature) lower than those expected for the production engine under ideal motored conditions, and they should not be transferred directly to the real engine.

The present results can be related to earlier work as follows. Payri et al. [2] found that RANS-based models predict the mean in-cylinder flow reasonably well around TDC, although turbulence can be under-predicted where squish effects are important. Experimental and numerical studies [3, 4] showed that the piston crown shape strongly influences the tumble ratio and the turbulent kinetic energy at the end of compression; since a flat piston was used here, the tumble structures in Figs. 12 and 13 provide a flat-piston baseline against which bowl geometries can be assessed. In contrast to [2–6], which used three-dimensional models to compare port or piston designs, the contribution of the present work is the same-geometry comparison of fixed and moving-boundary solutions combined with the motored thermodynamic analysis.

The study has limitations: the two-dimensional model cannot represent swirl or the three-dimensional structure of tumble; its effective volume ratio (about 12) is lower than the compression ratio of the production engine, so the peak values are lower than in the real engine; the inlet mass flow rate was taken from the three-dimensional engine and, in the planar model, is applied per unit depth, so the intake jet is weaker than in reality and the intake results should be regarded as qualitative; the valves are represented by fixed, fully open slots and the outlet pressure is imposed at the exhaust valve plane, so the cylinder pressure during the exhaust stroke is strongly underestimated; the standard k–ε model may under-predict turbulence in strongly compressed regions [2]; and the velocity fields have not yet been validated against measurements. These limitations will be addressed in future work with three-dimensional models and experimental data.

IV. CONCLUSION

A dynamic mesh CFD model was used to study the in-cylinder cold flow of a single-cylinder CI engine in three cases: fixed-geometry intake, intake and exhaust with piston motion, and motored compression and expansion. The main conclusions are as follows.

1. In the fixed geometry, the intake jet forms a single large toroidal vortex that controls the baseline flow structure.

2. With piston motion, the flow changes qualitatively: one dominant clockwise vortex and two smaller counter-rotating vortices form during intake, the flow becomes markedly asymmetric, and residual vortices remain in the cylinder at the end of the exhaust stroke. Moving boundaries are therefore essential for predicting the in-cylinder aerodynamics correctly.

3. During motored compression, the gauge pressure and temperature reach 3.176 MPa and 808.6 K near TDC, organized tumble motion and recirculation zones form, and the compression and expansion curves of the p–V diagram coincide. These values agree within 0.2 % with ideal isentropic compression at the effective volume ratio of the model (about 12), which verifies the thermodynamic consistency of the solution. For the compression ratio of 15.5 of the production engine, isentropic compression gives about 4.60 MPa and 898 K, so the absolute peak values of the planar model are lower than those of the real engine and should not be transferred to it directly.

4. The mesh-independent motored model provides a baseline for future studies that include fuel injection, spray dynamics, combustion and emission prediction; extending the model to three dimensions and validating it against measured velocity fields are the next steps.

5. The intake results were obtained with a constant inlet mass flow rate, which neglects the valve lift kinematics and the pressure difference across the intake valve, and the exhaust results were obtained with fixed, fully open valve slots and the outlet pressure imposed at the valve plane, which strongly underestimates the cylinder pressure during the exhaust stroke. These results are therefore qualitative: they describe the topology of the in-cylinder flow rather than its quantitative strength.

Table 4 Nomenclature

Symbol	Description, unit
$C_{1\varepsilon}$, $C_{2\varepsilon}$, C_{μ}	turbulence model constants
E	total specific energy, J/kg
G_k	production of turbulent kinetic energy, kg/(m·s^3)
k	turbulent kinetic energy, m^2/s^2
L	connecting rod length, m
n	polytropic exponent
p	pressure, Pa
R	specific gas constant, J/(kg·K)
r	crank radius, m
S	stroke, m
T	temperature, K
t	time, s
$\mathbf{u}$	velocity vector, m/s
V	cylinder volume, m^3
x_p	piston displacement from TDC, m
ε	turbulent dissipation rate, m^2/s^3
θ, θ_0	crank angle, initial crank angle, deg
λ	thermal conductivity, W/(m·K)
μ, μ_t, μ_{eff}	molecular, turbulent and effective viscosity, Pa·s
ρ	density, kg/m^3
σ_k, σ_ε	turbulent Prandtl numbers for k and ε
τ	viscous stress tensor, Pa
Φ	viscous dissipation term, W/m^3
ω	angular velocity of crankshaft, rad/s

Table 5Abbreviations

Abbreviation	Meaning
BDC	bottom dead center
CFD	computational fluid dynamics
CI	compression ignition
HCCI	homogeneous charge compression ignition
LES	large eddy simulation
PCCI	premixed charge compression ignition
RANS	Reynolds-averaged Navier–Stokes
RCCI	reactivity controlled compression ignition
TDC	top dead center

References

1. Heywood J.B. *Internal combustion engine fundamentals*. New York, McGraw-Hill, 1988. 930 p.
2. Payri F., Benajes J., Margot X., Gil A. CFD modeling of the in-cylinder flow in direct-injection diesel engines. *Computers & Fluids*, 2004, vol. 33, no. 8, pp. 995-1021. doi: 10.1016/j.compfluid.2003.09.003
3. Murali Krishna B., Mallikarjuna J.M. Comparative study of in-cylinder tumble flows in an internal combustion engine using different piston shapes – an insight using particle image velocimetry. *Experiments in Fluids*, 2010, vol. 48, no. 5, pp. 863-874. doi: 10.1007/s00348-009-0783-6
4. Gnana Sagaya Raj A.R., Mallikarjuna J.M., Ganesan V. Energy efficient piston configuration for effective air motion – a CFD study. *Applied Energy*, 2013, vol. 102, pp. 347-354. doi: 10.1016/j.apenergy.2012.07.022
5. Perini F., Miles P.C., Reitz R.D. A comprehensive modeling study of in-cylinder fluid flows in a high-swirl, light-duty optical diesel engine. *Computers & Fluids*, 2014, vol. 105, pp. 113-124. doi: 10.1016/j.compfluid.2014.09.011
6. Taghavifar H., Khalilarya S., Jafarmadar S. Engine structure modifications effect on the flow behavior, combustion, and performance characteristics of DI diesel engine. *Energy Conversion and Management*, 2014, vol. 85, pp. 20-32. doi: 10.1016/j.enconman.2014.05.076
7. Som S., Aggarwal S.K., El-Hannouny E.M., Longman D.E. Investigation of nozzle flow and cavitation characteristics in a diesel injector. *Journal of Engineering for Gas Turbines and Power*, 2010, vol. 132, no. 4, art. no. 042802. doi: 10.1115/1.3203146
8. Som S., Aggarwal S.K. Effects of primary breakup modeling on spray and combustion characteristics of compression ignition engines. *Combustion and Flame*, 2010, vol. 157, no. 6, pp. 1179-1193. doi: 10.1016/j.combustflame.2010.02.018
9. Postrioti L., Mariani F., Battistoni M. Experimental and numerical momentum flux evaluation of high pressure diesel spray. *Fuel*, 2012, vol. 98, pp. 149-163. doi: 10.1016/j.fuel.2012.03.043
10. Payri R., García-Oliver J.M., Xuan T., Bardi M. A study on diesel spray tip penetration and radial expansion under reacting conditions. *Applied Thermal Engineering*, 2015, vol. 90, pp. 619-629. doi: 10.1016/j.applthermaleng.2015.07.042
11. Kokjohn S.L., Hanson R.M., Splitter D.A., Reitz R.D. Experiments and modeling of dual-fuel HCCI and PCCI combustion using in-cylinder fuel blending. *SAE International Journal of Engines*, 2009, vol. 2, no. 2, pp. 24-39. doi: 10.4271/2009-01-2647
12. Kokjohn S.L., Hanson R.M., Splitter D.A., Reitz R.D. Fuel reactivity controlled compression ignition (RCCI): a pathway to controlled high-efficiency clean combustion. *International Journal of Engine Research*, 2011, vol. 12, no. 3, pp. 209-226. doi: 10.1177/1468087411401548
13. Benajes J., Molina S., García A., Monsalve-Serrano J. Effects of direct injection timing and blending ratio on RCCI combustion with different low reactivity fuels. *Energy Conversion and Management*, 2015, vol. 99, pp. 193-209. doi: 10.1016/j.enconman.2015.04.046
14. Reitz R.D., Duraisamy G. Review of high efficiency and clean reactivity controlled compression ignition (RCCI) combustion in internal combustion engines. *Progress in Energy and Combustion Science*, 2015, vol. 46, pp. 12-71. doi: 10.1016/j.pecs.2014.05.003
15. Zhou L., Luo K.H., Qin W., Jia M., Shuai S.J. Large eddy simulation of spray and combustion characteristics with realistic chemistry and high-order numerical scheme under diesel engine-like conditions. *Energy Conversion and Management*, 2015, vol. 93, pp. 377-387. doi: 10.1016/j.enconman.2015.01.033
16. Hamada K.I., Rahman M.M., Ramasamy D., Noor M.M., Kadirgama K. Numerical investigation of in-cylinder flow characteristics of hydrogen-fuelled internal combustion engine. *Journal of Mechanical Engineering and Sciences*, 2016, vol. 10, no. 1, pp. 1792-1802. doi: 10.15282/jmes.10.1.2016.4.0172
17. Zandie M., Ng H.K., Gan S., Muhamad Said M.F., Cheng X. A comprehensive CFD study of the spray combustion, soot formation and emissions of ternary mixtures of diesel, biodiesel and gasoline under compression ignition engine-relevant conditions. *Energy*, 2022, vol. 260, art. no. 125191. doi: 10.1016/j.energy.2022.125191
18. Gowrishankar S., Krishnasamy A. CFD analysis of combustion and emission characteristics of biodiesel under conventional and late-injection based premixed combustion conditions. *Fuel*, 2023, vol. 351, art. no. 129021. doi: 10.1016/j.fuel.2023.129021
19. Posch S., Gößnitzer C., Lang M., Novella R., Steiner H., Wimmer A. Turbulent combustion modeling for internal combustion engine CFD: a review. *Progress in Energy and Combustion Science*, 2025, vol. 106, art. no. 101200. doi: 10.1016/j.pecs.2024.101200
20. Jeong S.-J., Seo S., Moon S.-J. CFD simulation of pre-chamber spark-ignition large bore CNG engine: model development, practical applications, and experimental validation. *Energies*, 2025, vol. 18, no. 7, art. no. 1600. doi: 10.3390/en18071600

21. Kantaroğlu E. CFD-based analysis of performance and emissions in an i-DSI engine using various e-fuels and syngas. *Flow, Turbulence and Combustion*, 2025, vol. 115, pp. 781-827. doi: 10.1007/s10494-025-00660-9

22. Launder B.E., Spalding D.B. The numerical computation of turbulent flows. *Computer Methods in Applied Mechanics and Engineering*, 1974, vol. 3, no. 2, pp. 269-289. doi: 10.1016/0045-7825(74)90029-2

Information about authors.



Dr. Mehul P. Bambhania

Mechanical Engineering Department, FTE, The Maharaja Sayajirao University of Baroda, Vadodara, India.

Research interests: Cavitation, Bio-fuel, CFD.

ORCID: https://orcid.org/0000-0001-7910-5881

E-mail: mehulbambhania-med@msubaroda.ac.in



Mr. Deepak S. Jani

Mechanical Engineering Department, Gyanmanjari Institute of Technology, Bhavnagar, India.

Research interests: Heat transfer, Nano fluid.

ORCID: https://orcid.org/0009-0008-6304-7347
E-mail: janideepak5457@gmail.com



Mr. Jani Dhruvkumar Manishkumar

Mechanical Engineering Department, FTE, The Maharaja Sayajirao University of Baroda, Vadodara, India.

Research interests: CAD-CAM.

ORCID: https://orcid.org/0009-0000-9345-8149

E-mail: dhruv.jani-med@msubaroda.ac.in